On computing the physical sources of jet noise

S. Sinayoko*, A. Agarwal†
Institute of Sound and Vibration Research, University of Southampton

We derive a closed system of equations that relates the acoustically radiating flow variables to the sources of sound for homentropic flows. We use radiating density, momentum density and modified pressure as the dependent variables which leads to simple source terms for the momentum equations. The source terms involve the non-radiating parts of the density and momentum density fields. These non-radiating components are obtained by removing the radiating wavenumbers in the Fourier domain. We demonstrate the usefulness of this new technique on an axi-symmetric jet solution of the Navier–Stokes equations, obtained by direct numerical simulation (DNS). The dominant source term is proportional to the square of the non-radiating part of the axial momentum density. We compare the sound sources to that obtained by an acoustic analogy and find that they have more realistic physical properties. Their frequency content and amplitudes are consistent with . We validate the sources by computing the radiating sound field and comparing it to the DNS solution.

I. Introduction

Despite more than 50 years of research in aeroacoustics, controlling the sound radiated by turbulent jets remains difficult. One reason is that no definite answer has been found on how turbulent flows generate sound. A major obstacle is the lack of understanding of the physical sources of sound in a jet.

One way to derive the aerodynamic noise sources is to use an acoustic analogy. In an acoustic analogy, the hydrodynamic field is assumed to be independent from the acoustic field. This allows to rearrange the Navier-Stokes equations to have a linear wave-propagation operator on the left-hand side; the remaining terms are grouped as sources on the right hand side. In general, the operator is obtained by deriving the governing equations for the flow fluctuations about a steady mean-flow. Goldstein[1] provides a good generalisation of such approaches. The fluctuating variables on the left-hand-side are the dependent variables of the problem and represent both acoustic and hydrodynamic waves. This implies that the sources on the right-hand side cannot be identified as just sound sources. Furthermore, we expect the sound field to be a small by-product of the hydrodynamic field. Therefore, the sound source should be a function of the hydrodynamic field only. This property is not satisfied by traditional acoustic analogies.

An attempt to overcome these difficulties and to define the physical sources of sound is made by Goldstein.[2] He shows that if a flow field can be separated into its radiating and non-radiating components, then the resulting sound sources are mainly a function of the non-radiating components and should approach the physical sources of sound. The present paper is inspired by Goldstein's work. Our objective is to show that it is indeed possible to separate radiating acoustic components from non-radiating components in nonlinear flows.

We show that, following such a decomposition, the sound sources depend only on the non-acoustic field. The source terms do not contain the dependent acoustic variables and should therefore represent the true sources of sound. We present a simple expression for the source terms. It is similar to the one derived by Goldstein. However, our result is only approximate because we ignore entropy sources and terms which are quadratic in the acoustic variables. These choices simplify the derivation of the sources and should have little consequence for the flows we are studying here. We also derive the noise sources associated with a time-averaged base flow. We validate the results by propagating the sound sources we obtain with a Linearized Euler equations solver.

*PhD student, ISVR, University of Southampton
†Lecturer, ISVR, University of Southampton

The paper is organised as follows. In section 2, we derive the aerodynamic noise sources in two different ways. The first one is based on a non-radiating unsteady base flow. The second one relies on a time-averaged base flow. We restrict ourselves to homentropic flows. In section III, we decompose an axisymmetric jet into its radiating part and non-radiating part by using a convolution filter.[3] The axisymmetric jet is excited at the inflow by two frequencies and satisfies an inhomogeneous version of the Navier-Stokes equations. The non-radiating base flow is used to compute the corresponding sound sources. We then propagate the sound sources and compare the radiating acoustic field with the one present in the original flow field.

II. Derivation of the noise sources

We derive the noise sources by decomposing the flow variables into two parts: a base part and a fluctuating part. The base flow must be such that the fluctuating part corresponds to sound waves in the far-field. We then linearize the flow equations to obtain the governing equations for the fluctuating variables. These governing equations are inhomogeneous. The left hand side is linear in the fluctuating variables, and the right hand side corresponds to the noise sources. The underlying assumption is that sound generation and sound propagation are decoupled. The properties of the noise sources depend on the choice of base flow.

A. Noise sources based on a silent base flow

Flow decomposition

We decompose the flow field into its radiating and non-radiating components. The radiating components are those which satisfy the dispersion relation $|\mathbf{k}| = |\omega|/c_\infty$ in the frequency–wavenumber domain, where $\mathbf{k}$ is the wavenumber, ω the angular frequency and c_∞ the far field speed of sound (Crighton,[4] Goldstein[2]). Physically, the non-radiating components are made of:

- the steady mean flow,
- the hydrodynamic fluctuations about the mean flow.

The radiating components correspond to acoustic waves. In this paper, we use the terms "acoustic field" and "radiating field" interchangeably.

For a given flow variable q, the non-radiating part $\overline{q}$ can be obtained by using a convolution filter g, i.e.

$$\overline{q}(\mathbf{x},t) \equiv \int_{-\infty}^{+\infty} \int_{\mathcal{V}} g(\mathbf{y},\tau) q(\mathbf{x}-\mathbf{y}, t-\tau)\, d^3\mathbf{y}\, d\tau, \tag{1}$$

where $\mathcal{V}$ denotes the entire spatial domain. To achieve this, the convolution filter must satisfy

$$G(\mathbf{k},\omega) = \begin{cases} 0 & \text{if} \quad |\mathbf{k}| = |\omega|/c_\infty, \\ 1 & \text{if} \quad |\mathbf{k}| \neq |\omega|/c_\infty, \end{cases} \tag{2}$$

where G is the four-dimensional Fourier transform of g, defined as

$$G(\mathbf{k},\omega) \equiv \int_{-\infty}^{+\infty} \int_{\mathcal{V}} g(\mathbf{x},t) e^{i(\omega t - \mathbf{k}\cdot\mathbf{x})}\, d^3\mathbf{x}\, dt. \tag{3}$$

The flow variable q can then be written as

$$q = \overline{q} + q', \tag{4}$$

where q' represents the radiating components of the flow.

Source definition

The flow variables satisfy the Navier–Stokes equations:

$$\frac{\partial \rho}{\partial t} + \frac{\partial}{\partial x_j} \rho v_j = 0, \tag{5}$$

$$\frac{\partial}{\partial t} \rho v_i + \frac{\partial}{\partial x_j} \rho v_i v_j + \frac{\partial p}{\partial x_i} = \frac{\partial}{\partial x_j} \sigma_{ij}, \tag{6}$$

where ρ, p and $\mathbf{v} = (v_i)$ denote the density, pressure and flow velocity, and σ_{ij} the viscous stress tensor. We assume that the flow is homentropic so that $\sigma_{ij} = 0$. For a perfect gas, we can write the energy equation as (Goldstein[5])

$$\frac{\partial p}{\partial t} + v_j \frac{\partial p}{\partial x_j} + \gamma p \frac{\partial v_j}{\partial x_j} = 0. \tag{7}$$

Introducing the variable $\pi \equiv p^{1/\gamma}$ allows us to rewrite (6) and (7) as (Lilley[6])

$$\frac{\partial}{\partial t}\rho v_i + \frac{\partial}{\partial x_j}\rho v_i v_j + \frac{\partial}{\partial x_i}\pi^\gamma = 0, \tag{8}$$

$$\frac{\partial \pi}{\partial t} + \frac{\partial}{\partial x_j}\pi v_j = 0. \tag{9}$$

Note that the equation for pressure is now in conservative form.

Let $\mathcal{L}$ denote the linear operator associated with the convolution filter of (1). For each term in the above equations, the radiating part can be obtained by applying the linear filter $\mathcal{L}' \equiv \mathcal{I} - \mathcal{L}$, where $\mathcal{I}$ denotes the identity operator. Applying $\mathcal{L}'$ to (5), (8) and (9) gives the governing equations for the radiating components, we get

$$\frac{\partial \rho'}{\partial t} + \frac{\partial}{\partial x_j}\left(\rho v_j\right)' = 0, \tag{10}$$

$$\frac{\partial}{\partial t}\left(\rho v_i\right)' + \frac{\partial}{\partial x_j}\left(\rho v_i v_j\right)' + \frac{\partial}{\partial x_i}\left(\pi^\gamma\right)' = 0, \tag{11}$$

$$\frac{\partial \pi'}{\partial t} + \frac{\partial}{\partial x_j}\left(\pi v_j\right)' = 0. \tag{12}$$

We rewrite each of the above equations to obtain an operator that is linear in the radiating dependent variables $\{\rho'$, $(\rho v_i)'$ and $\pi'\}$ on the left-hand side.

In (11), the term $\rho v_i v_j$ can be expanded as

$$\rho v_i v_j = \frac{\rho v_i \rho v_j}{\rho} = \frac{\overline{\rho v_i}\,\overline{\rho v_j}}{\overline{\rho}} + \frac{\overline{\rho v_j}}{\overline{\rho}}\left(\rho v_i\right)' + \frac{\overline{\rho v_i}}{\overline{\rho}}\left(\rho v_j\right)' - \frac{\overline{\rho v_i}\,\overline{\rho v_j}}{\overline{\rho}^2}\rho' + O(\rho'^2), \tag{13}$$

$$\rho v_i v_j = \overline{\rho}\,\widetilde{v}_i\widetilde{v}_j + \widetilde{v}_j\left(\rho v_i\right)' + \widetilde{v}_i\left(\rho v_j\right)' - \widetilde{v}_i\widetilde{v}_j\rho' + O(\rho'^2), \tag{14}$$

where we have introduced

$$\widetilde{v}_i = \frac{\overline{\rho v_i}}{\overline{\rho}}, \tag{15}$$

so that $\widetilde{v}_i$ represents Favre-averaged v_i, and where $O(\rho'^2)$ represents terms that are at least quadratic in the radiating variables. Because the radiating part of the flow is normally several orders of magnitude smaller than the non-radiating part, these higher order terms are expected to be small and will be neglected. Applying $\mathcal{L}'$ to (14) gives

$$\left(\rho v_i v_j\right)' \approx \underbrace{\left(\overline{\rho}\,\widetilde{v}_i\widetilde{v}_j\right)'}_{\text{(b)}} + \underbrace{\left(\widetilde{v}_j(\rho v_i)' + \widetilde{v}_i(\rho v_j)' - \widetilde{v}_i\widetilde{v}_j\rho'\right)'}_{\text{(a)}}. \tag{16}$$

We assume a one-way coupling between hydrodynamics and acoustics: the hydrodynamic field is responsible for the production of sound but the sound field does not affect the hydrodynamic field. The source of sound must therefore be independent of the radiating components. The only terms satisfying this requirement are those in group (b), which are non-linear in hydrodynamic quantities. The terms in group (a) involve an acoustic component interacting with the non-radiating base flow. These terms represent propagation effects such as refraction and can be excluded from the source. The other non-linear term in (11) is $\left(\pi^\gamma\right)'$ which can be decomposed as follows:

$$\pi^\gamma = (\overline{\pi} + \pi')^\gamma = \overline{\pi}^\gamma + \gamma\overline{\pi}^{\gamma-1}\pi' + O(\pi'^2), \tag{17}$$

$$\left(\pi^\gamma\right)' \approx \underbrace{\left(\overline{\pi}^\gamma\right)'}_{(b)} + \underbrace{\left(\gamma\overline{\pi}^{\gamma-1}\pi'\right)'}_{(a)}. \tag{18}$$

However, since the flow is homentropic, we have

$$p = \frac{p_\infty}{\rho_\infty^\gamma}\rho^\gamma. \tag{19}$$

where p_∞ and ρ_∞ denote the the ambient pressure and ambient density respectively. Identifying the dominant terms in (19) leads to

$$\overline{p} = \frac{p_\infty}{\rho_\infty^\gamma}\overline{\rho}^\gamma. \tag{20}$$

From (19), we also have

$$\pi \equiv p^{1/\gamma} = \frac{\pi_\infty}{\rho_\infty}\,\rho, \tag{21}$$

Applying $\mathcal{L}$ and $\mathcal{L}'$ to (21) gives

$$\overline{\pi} = \frac{\pi_\infty}{\rho_\infty}\overline{\rho}, \quad \pi' = \frac{\pi_\infty}{\rho_\infty}\rho'. \tag{22}$$

From (22) and (20), we can write

$$(\,\overline{\pi}^\gamma\,)' = \frac{\pi_\infty}{\rho_\infty}\,(\,\overline{\rho}^\gamma\,)' = \left(\frac{\rho_\infty}{\pi_\infty}\right)^{\gamma-1}(\,\overline{p}\,)' = 0, \tag{23}$$

so the source term (b) of equation (18) is equal to zero for a homentropic flow.

Similarly, in equation (12), $(\,\pi v_j\,)'$ can be decomposed as follows

$$(\,\pi v_j\,)' \approx \underbrace{(\,\overline{\pi}\widetilde{v_j}\,)'}_{(b)} + \underbrace{\left(\frac{\overline{\pi}}{\overline{\rho}}\,(\,\rho v_j\,)' + \widetilde{v_j}\pi' - \frac{\overline{\pi}}{\overline{\rho}}\widetilde{v_j}\rho'\right)'}_{(a)} \tag{24}$$

From (22) and (15) it can be seen that

$$(\,\overline{\pi}\widetilde{v_j}\,)' = \frac{\pi_\infty}{\rho_\infty}\,(\,\overline{\rho}\widetilde{v_j}\,)' = \frac{\pi_\infty}{\rho_\infty}\,(\,\overline{\rho v_j}\,)' = 0, \tag{25}$$

so the source term (b) in equation (24) is equal to zero.

We can now rewrite equations (10–12) by pushing the sound sources (b) of equations (16, 18) to the right hand side, and leaving the interaction terms (a) on the left hand side, which gives

$$\frac{\partial\rho'}{\partial t} + \frac{\partial}{\partial x_j}\,(\,\rho v_j\,)' = 0, \tag{26}$$

$$\frac{\partial}{\partial t}\,(\,\rho v_i\,)' + \frac{\partial}{\partial x_j}\,(\,\widetilde{v_j}(\rho v_i)' + \widetilde{v_i}(\rho v_j)' - \widetilde{v_i}\widetilde{v_j}\rho'\,)' + \gamma\frac{\partial}{\partial x_i}\left(\,\overline{\pi}^{\gamma-1}\pi'\,\right)' = f_{1i}, \tag{27}$$

$$\frac{\partial\pi'}{\partial t} + \frac{\partial}{\partial x_j}\left(\frac{\overline{\pi}}{\overline{\rho}}((\,\rho v_j\,)' - \widetilde{v_j}\rho') + \widetilde{v_j}\pi'\right)' = 0, \tag{28}$$

where the momentum equation source term f_{1i} is defined as

$$f_{1i} \equiv -\frac{\partial}{\partial x_j}\,(\,\overline{\rho}\,\widetilde{v_i}\widetilde{v_j}\,)'\,. \tag{29}$$

The equation shows that the noise source f_{1i} is a radiating quantity; this is what we expect because the operator on the left hand side of (26–28) is linear in the radiating variables. This means that f_{1i} produces only acoustic waves. Also, as we expect, the source is expressed as a (nonlinear) function of only the non-radiating components: it is free of the dependant (acoustic) variables. Therefore, this source should represent the true source of aerodynamically generated sound. These key features distinguish the present source from past representations based on acoustic analogies.

B. Noise sources based on a steady base flow

A simpler flow decomposition method is to use a time averaged base flow. Any flow variable q is decomposed as

$$q = q_0 + q'' \tag{30}$$

where q_0 and q'' denote respectively the steady and unsteady part of q.

Since taking the time average is a linear operation, following the procedure of section A leads to

$$\frac{\partial \rho''}{\partial t} + \frac{\partial (\rho v_j)''}{\partial x_j} = 0, \tag{31}$$

$$\frac{\partial (\rho v_i)''}{\partial t} + \frac{\partial (\rho v_i v_j)''}{\partial x_j} + p_\infty \frac{\partial (\pi^\gamma)''}{\partial x_i} = 0, \tag{32}$$

$$\frac{\partial \pi''}{\partial t} + \gamma \frac{\partial (\pi v_j)''}{\partial x_j} = 0. \tag{33}$$

The term $\rho v_i v_j$ can be decomposed as

$$\rho v_i v_j = \frac{\rho v_i \, \rho v_j}{\rho} = \begin{cases} (a) & \rho_0 \widehat{v_i} \widehat{v_j} + \\ (b) & \widehat{v_j} \, (\, \rho v_i \,)'' + \widehat{v_i} \, (\, \rho v_j \,)'' - \widehat{v_i} \widehat{v_j} \rho'' + \\ (c) & \dfrac{1}{\rho_0} \, (\, \rho v_i \,)'' \, (\, \rho v_j \,)'' - \dfrac{\widehat{v_j}}{\rho_0} \, (\, \rho v_i \,)'' \, \rho'' - \dfrac{\widehat{v_i}}{\rho_0} \, (\, \rho v_j \,)'' \, \rho'' + \dfrac{\widehat{v_i} \, \widehat{v_j}}{\rho_0} \rho''^2 + O(\rho''^3), \end{cases} \tag{34}$$

where we have introduced

$$\widehat{v_i} = \frac{(\, \rho v_i \,)_0}{\rho_0}, \tag{35}$$

which is analogous to $\widetilde{v_i}$ but uses a steady base flow rather than a non-radiating base flow. We then retain the unsteady part of (34) and identify the noise sources. The terms $(a - c)$ behave as follows:

(a) is steady, i.e. $(a)'' = 0$,

(b) is purely unsteady, i.e. $(b)'' = (b)$, and corresponds to interaction between the mean flow and the fluctuating flow,

(c) is non-linear in unsteady variables and contains the sound sources.

The term $(\, \pi^\gamma \,)''$ is decomposed as follows:

$$\pi^\gamma = (\pi_0 + \pi'')^\gamma = \pi_0^\gamma + \gamma \pi_0^{\gamma - 1} \pi'' + \frac{1}{2} \gamma (\gamma - 1) \pi_0^{\gamma - 2} \pi''^2 + O(\pi''^3) \tag{36}$$

$$(\, \pi^\gamma \,)'' \approx \gamma \pi_0^{\gamma - 1} \pi'' + \frac{1}{2} \gamma (\gamma - 1) \pi_0^{\gamma - 2} (\pi''^2)''. \tag{37}$$

Finally, the term πv_j is decomposed as follows:

$$\pi v_j = \frac{\pi \rho v_j}{\rho} = \begin{cases} (a) & \dfrac{\pi_0}{\rho_0} \, (\, \rho v_j \,)_0 + \\ (b) & \dfrac{\pi_0}{\rho_0} \, (\, \rho v_j \,)'' + \widehat{v_j} \pi'' - \dfrac{\pi_0}{\rho_0} \widehat{v_j} \rho'' + \\ (c) & \dfrac{1}{\rho_0} \pi'' \, (\, \rho v_j \,)'' - \dfrac{\widehat{v_j}}{\rho_0} \rho'' \pi'' - \dfrac{\pi_0}{\rho_0^2} \rho'' \, (\, \rho v_j \,)'' + \dfrac{\pi_0 \widehat{v_j}}{\rho_0^2} \rho''^2 + O(\rho''^3), \end{cases} \tag{38}$$

where (a) has no unsteady part, (b) corresponds to interaction terms and (c) to source terms. However, (c) can be expressed as

$$\frac{1}{\rho_0} \left(\pi'' - \frac{\pi_0}{\rho_0} \rho'' \right) \left((\, \rho v_j \,)'' - \rho'' \widehat{v_j} \right). \tag{39}$$

Rewriting equations (22) and (20) for a time-averaged flow, we have

$$\pi'' = \frac{\pi_\infty}{\rho_\infty} \rho'' = \frac{\pi_0}{\rho_0} \rho'', \tag{40}$$

so (c) is equal to zero.

We can now rewrite equations (31–33) by pushing the sound sources to the right hand side and leaving the propagation terms on the left hand side:

$$\frac{\partial \rho''}{\partial t} + \frac{\partial}{\partial x_j}\left(\,\rho v_j\,\right)'' = 0, \tag{41}$$

$$\frac{\partial}{\partial t}\left(\,\rho v_i\,\right)'' + \frac{\partial}{\partial x_j}(\widehat{v_j}\left(\,\rho v_i\,\right)'' + \widehat{v_i}\left(\,\rho v_j\,\right)'' - \widehat{v_i}\widehat{v_j}\rho'') + \gamma\frac{\partial}{\partial x_i}\pi_0^{\gamma-1}\pi'' = f_{2i}, \tag{42}$$

$$\frac{\partial \pi''}{\partial t} + \frac{\partial}{\partial x_j}\left(\frac{\pi_0}{\rho_0}\left(\,\rho v_j\,\right)'' + \widehat{v_j}\pi'' - \frac{\pi_0}{\rho_0}\widehat{v_j}\rho''\right) = 0, \tag{43}$$

where the momentum equation source term f_{2i} is defined as

$$\begin{aligned} f_{2i} \equiv -\frac{\partial}{\partial x_j}\left(\frac{1}{\rho_0}\left(\,\rho v_i\,\right)''\left(\,\rho v_j\,\right)'' - \frac{\widehat{v_j}}{\rho_0}\left(\,\rho v_i\,\right)''\rho'' - \frac{\widehat{v_i}}{\rho_0}\left(\,\rho v_j\,\right)''\rho'' + \frac{\widehat{v_i}\,\widehat{v_j}}{\rho_0}\rho''^2\right) \\ -\frac{1}{2}\gamma(\gamma-1)\frac{\partial}{\partial x_i}\left(\pi_0^{\gamma-2}\left(\,\pi\,\right)''^2\right)'' \end{aligned} \tag{44}$$

III. Sources of sound in an axi-symmetric jet flow

A. Problem description

We now consider a nonlinear problem in which an axi-symmetric jet is excited by two discrete-frequency axi-symmetric disturbances at the jet exit. The frequencies are chosen to trigger some instability waves in the flow. These instability waves grow downstream and interact non-linearly, generating acoustic waves. The Mach number of the jet is 0.9 and the Reynolds number is 3600. The base mean flow is chosen to match the experimental data of Stromberg *et al.*[7]

Suponitsky and Sandham[8] performed direct numerical simulations of the compressible Navier–Stokes equations for this problem. In their simulations the mean flow was prescribed by imposing time-independent forcing terms. They ran simulations with different combinations of excitation frequencies and amplitudes. The data used here corresponds to the combination with the largest acoustic radiation. The two excitation frequencies are $\omega_1 = 2.4$ and $\omega_2 = 3.4$. The results presented in this section have been normalised by using the jet diameter D, jet exit speed U_j and the ambient density as the length, velocity and density scales, respectively.

B. Flow decomposition

In order to apply the convolution filtering technique for flow decomposition, we first need to obtain the Fourier transform (FT) of the flow field. In general this involves transforming in four (time and 3 space) dimensions. However, given the axi-symmetric nature of the present problem, we are able to do the spatial transforms in two dimensions: by applying a Hankel transform (HT) in the radial direction and a Fourier transform in the axial direction. The Hankel transform is carried out numerically by using the quasi-discrete Hankel transform described by Guizar-Sicairos and Guitiérrez-Vega.[9]

For a given flow variable q, the algorithm for obtaining the non-radiating variable $\overline{q}$ is as follows:

- interpolate and zero pad the data (to avoid aliasing) in the physical space,
- compute and remove the time-averaged variable q_0
- compute the FT in the axial direction and the HT in the radial direction,
- multiply by the filter window G,
- compute the inverse Hankel transform and the inverse Fourier transform,
- unpad the data and add back q_0.

Mathematically, the filtering procedure can be written as

$$\overline{q} = q_0 \quad + \quad \mathrm{HT}^{-1} \circ \mathrm{FT}^{-1}\Big(\mathrm{HT} \circ \mathrm{FT}(q - q_0) \times G\Big) \tag{45}$$

In the above equation, if q is the radial momentum ρv_r, then HT denotes the Hankel transform of order 1. Otherwise, HT denotes the Hankel transform of order 0.

The window G should satisfy equation (2). For a given frequency ω, we want G to have a value of 0 in a narrow band around $|\mathbf{k}| = |\omega|/c_\infty = k_{co}$ and of 1 everywhere else. We use a narrow Butterworth band-reject filter to achieve this:

$$G(\mathbf{k}) = \left(1 + \frac{|\mathbf{k}|\sigma}{|\mathbf{k}|^2 - k_{co}^2}\right)^{-4}, \tag{46}$$

where σ controls the width of the stop-band and k_{co} is the cut-off frequency. In the present problem, the noise radiates mainly at the difference frequency, $\Delta w = \omega_2 - \omega_1$. For this frequency, $k_{co} = 1.2$. We choose a value of 0.25 for σ.

Results and discussion

The success of the filtering operation is verified by examining the fluctuating part of the acoustic field ($\pi' = \pi - \overline{\pi}$), which should contain no hydrodynamic components. Figures 1(a) and 1(b) respectively show total pressure π (excluding low frequency components π_0), and fluctuating pressure π'. They demonstrate that a clear identification of the radiating components has been achieved since π' contains no hydrodynamic component. This shows that using this filtering procedure we are able to obtain the filtered field to a very high order of accuracy because we are subtracting two large quantities (π and $\overline{\pi}$) to obtain a much smaller quantity (π'). More precisely, we find that π' is three orders of magnitude smaller than $\overline{\pi}$ along the jet centerline, and $\pi_h = \overline{\pi} - \pi_0$ is two orders of magnitude smaller than π_0. Similar results have been obtained using the same filter for the other flow variables. This validates the hypotheses that acoustics are much smaller than hydrodynamics, and hydrodynamics are much smaller than time-averaged components.

The above filtering procedure is equivalent to convolving the flow with a mask. In the vicinity of the boundary, a part of the mask will lie outside the computational domain where the flow is set to zero due to zero-padding. This leads to inaccuracies near boundaries. To restrict this effect to small regions, the filter must be narrow in the space–time domain. Unfortunately, optimal non-radiating filters must also be narrow in the wavenumber–frequency domain, which is impossible. A trade-off must be made between these two requirements. As can be seen in figure 1, π' is over-estimated in the first 4 jet diameters. One possible solution would be to extend the computational domain upstream in the simulations.

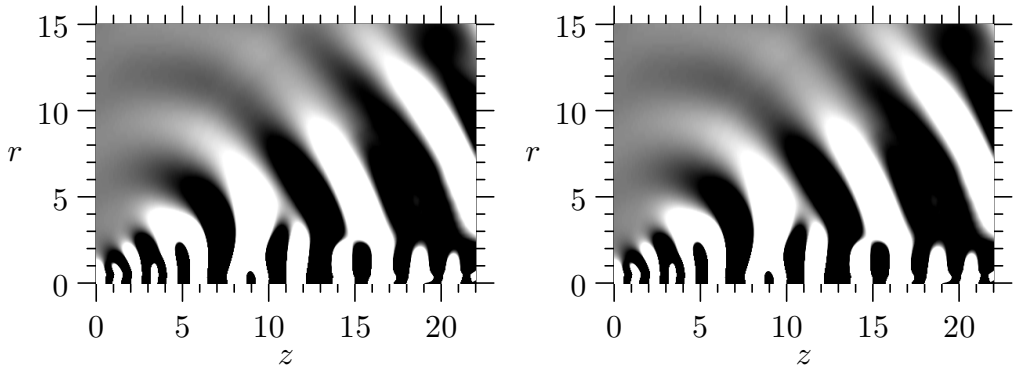

(a) Total pressure π (b) Fluctuating pressure $\pi' = \pi - \overline{\pi}$

Figure 1: Pressure fields for a single time frame. In (a), low frequency components p_0 have been removed for plotting. The linear contour scale ranges from $-5 \cdot 10^{-6}$ (black) to $5 \cdot 10^{-6}$ (white).

C. Sound sources

We compute the dominant terms in the axial momentum sources f_{1z} and f_{2z} of equations (29, 44), i.e

$$f_{1z} = \frac{\partial}{\partial z}\overline{\rho}\widetilde{v_z}\widetilde{v_z}, \quad f_{2z} = \frac{\partial}{\partial z}\rho_0 v_z'' v_z''. \tag{47}$$

Figure 2(a) shows an instantaneous contour plot of f_{1z} in the physical domain for $0 \leq r \leq 6.0$ and $0 \leq z \leq 17$. Figure 2(b) shows a similar contour plot for f_{2z} for $0 \leq r \leq 3.0$ and $0 \leq z \leq 17$. The source distribution

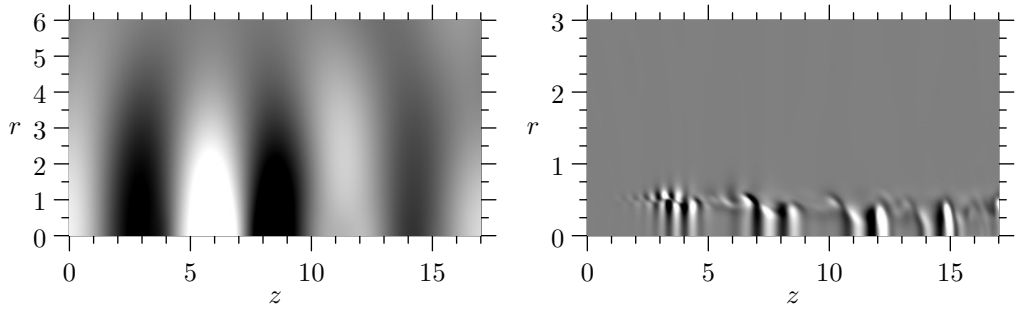

(a) Sound source f_{1z} associated with a non-radiating base flow.

(b) Sound source f_{2z} associated with a time-averaged base flow.

Figure 2: Sound sources for a single time frame. The contour scale ranges from $-1 \cdot 10^{-5}$ (black) to $1 \cdot 10^{-5}$ (white) in (a) and $-5 \cdot 10^{-3}$ (black) to $5 \cdot 10^{-3}$ (white) in (b).

is different in the two cases. With the non-radiating base flow, the source f_{1z} is spread over the first 4 jet diameters in the radial direction, and peaks around $z = 6$ in the axial direction, which corresponds to the end of the potential core. The source decays for $z >= 10$. With the time averaged base flow, the source f_{2z} is distributed within the jet ($r < 0.5$) and around the shear layer ($r = 0.5$). In terms of amplitude, the peak value of f_{2z} is three orders of magnitude greater than that of f_{1z}. This can be explained as follows: since f_{1z} is purely radiating (from (29)), it does not contain any hydrodynamic component, which is not the case of f_{2z}. These hydrodynamic components are also three orders of magnitude greater than the acoustic components, as explained in section B. The source f_{2z} drives both hydrodynamics and acoustics, whereas f_{1z} only generates acoustics. Furthermore, f_{1z} exhibits mostly some relatively large structures of the order of the acoustic wavelength $2\pi/\Delta\omega = 5.2$, while f_{2z} involves smaller structures.

Further physical insight can be obtained by looking at the power spectral density (PSD) of those sources. Figure 3(a) shows the PSD of source f_{1z} for $r = 0$, where f_{1z} is maximum as can be seen in figure 2(a). Figure 3(b) shows the PSD of f_{2z} for $r = 0.25$, where f_{2z} is dominant. These figures indicate that f_{1z} is dominated by the frequency $\Delta\omega = 1.2$, whereas f_{2z} contains several other frequencies, e.g. $\omega_1 = 2.2$, $\omega_2 = 3.4$, $2\omega_1 = 4.4$ and $\omega_1 + \omega_2 = 5.6$. We expect the true source of sound to have the frequency of acoustic waves, i.e. $\Delta\omega$. In that respect, the source f_{1z} based on a non-radiating base flow is more physical than f_{2z} which is based on a time-averaged base flow. Only a small portion of f_{2z} generates acoustic waves.

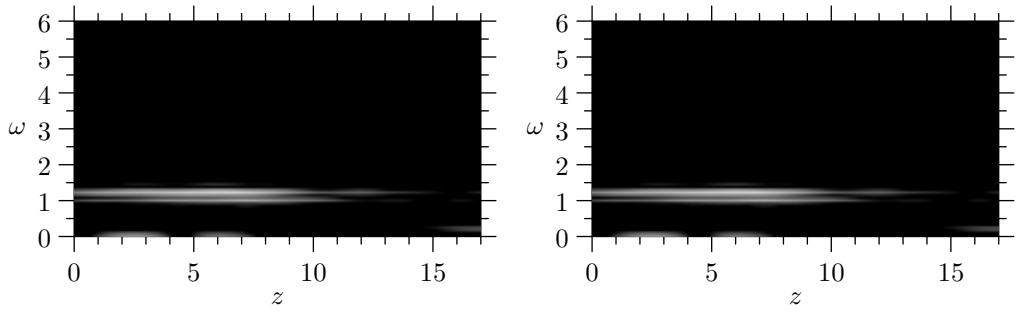

(a) (b)

Figure 3: Power spectral density for: (a) Source f_{1z} (non-radiating base flow) along $r = 0$, (b) Source f_{2z} (time-averaged base flow) along $r = 0.25$. The contour scale ranges from -85dB (black) to -65dB (white) in (a) and -50dB (black) to -20dB (white) in (b).

D. Validation

To validate the sound sources, we compute the sound they generate by solving equations (26–28) and (41–43). For source f_{1z}, we assume that the linear operator on the left hand side of the governing equations (26–28)

can be approximated by the linearized Euler operator.

We solve the equations with a time-domain finite-difference solver that uses the Dispersion Relation Preserving scheme of Tam and Webb.[10] Since we know the frequency of the radiating waves, which corresponds to the difference frequency $\Delta\omega$, we express the sound sources in the time-domain as

$$f_z(t, \pm\Delta\omega) = F_z(\Delta\omega)e^{-i\Delta\omega t} + F_z(-\Delta\omega)e^{i\Delta\omega t} \tag{48}$$

$$f_z(t, \pm\Delta\omega) = 2\mathcal{R}\left\{F_z(\Delta\omega)\right\}\cos(\Delta\omega t) + 2\mathcal{I}\left\{F_z(\Delta\omega)\right\}\sin(\Delta\omega t), \tag{49}$$

where F_z is the time Fourier transform defined as

$$F_z(\omega) = \int_{-\infty}^{+\infty} f_z(t)e^{i\omega t}\,dt, \tag{50}$$

and $\mathcal{R}\{\}$ and $\mathcal{I}\{\}$ denote the real and imaginary parts respectively.

Figure 4(a) gives a snapshot of $f_{1z}(\Delta\omega)$: as expected it is very similar to the plot of f_{1z} shown in figure 2(a), since f_{1z} is largely dominated by frequency $\Delta\omega$ (figure 3(a)). A profile of $f_{1z}(\Delta\omega)$ is shown in figure 4(b). Similarly, the source $f_{2z}(\Delta\omega)$ used in the calculation is shown in figures 4(c) and 4(d). Note that f_{2z} is still two orders of magnitude larger than f_{1z} because of the presence of hydrodynamic components.

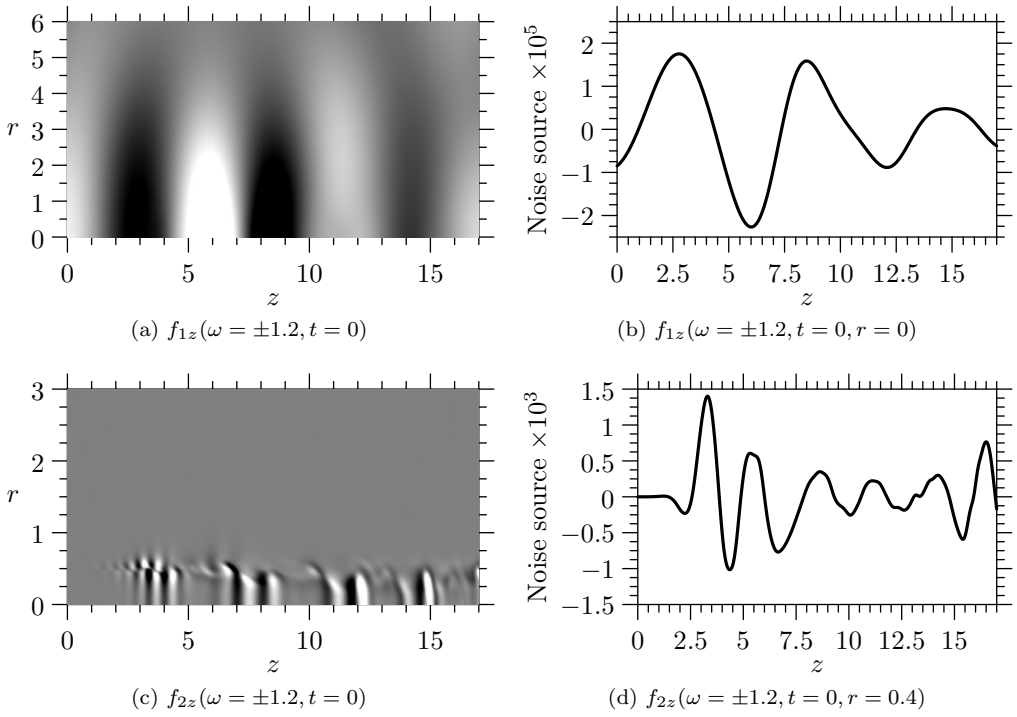

(a) $f_{1z}(\omega = \pm 1.2, t = 0)$ (b) $f_{1z}(\omega = \pm 1.2, t = 0, r = 0)$

(c) $f_{2z}(\omega = \pm 1.2, t = 0)$ (d) $f_{2z}(\omega = \pm 1.2, t = 0, r = 0.4)$

Figure 4: Noise sources at frequency $\omega = 1.2$ and time $t = 0$, contour plot (left) and profile (right): (top) Source $f_{1z}(\omega = \pm 1.2, t = 0)$ (non-radiating base flow), (bottom) Source $f_{2z}(\omega = \pm 1.2, t = 0)$ (time-averaged base flow). The contour scale ranges from $-1 \cdot 10^{-5}$ (black) to $1 \cdot 10^{-5}$ (white) in (a) and $-5 \cdot 10^{-4}$ (black) to $5 \cdot 10^{-4}$ (white) in (c).

The radiated pressure fields π' obtained by exciting the time averaged-flow with sources $f_{1z}(t, \pm\Delta\omega)$ and $f_{2z}(t, \pm\Delta\omega)$ are plotted in figure 5(a) and 5(b) respectively. The two solutions are in good agreement with each other in the acoustic region ($r >= 3$). The main differences occur close to the jet axis within the buffer zones of the simulations, $z <= 5$ and $z >= 17$, wherein sound waves are prevented from entering the computational domain. It can be seen that the solution generated by source f_{1z} is purely acoustic whereas the solution generated by source f_{2z} contains hydrodynamic components. The two solutions are compared with the value of the DNS solution at the radiating frequency $\pi(t, \pm\Delta\omega)$. The agreement is good which validates the source definitions of section II.

A quantitative comparison is shown in figure 6 where profiles of the three solutions are plotted along the line $r = 10$. The good agreement confirms that the axial momentum term $\partial(\overline{\rho}\widetilde{v_z}\widetilde{v_z})/\partial z$ is responsible for most of the sound generation.

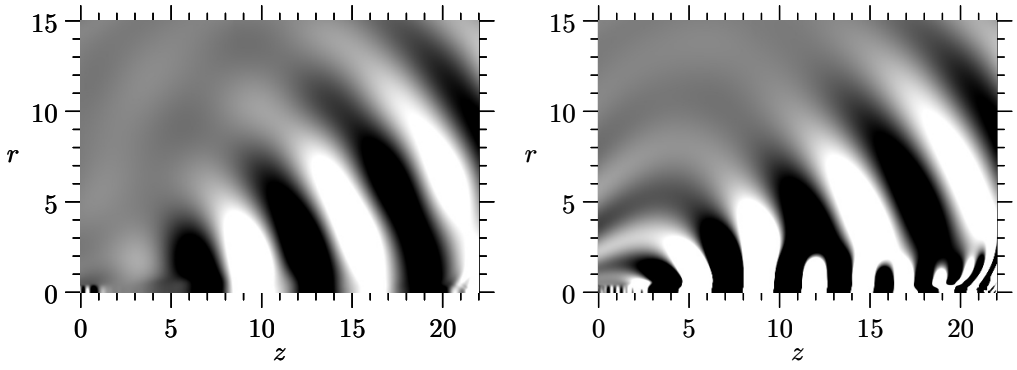

(a) Snapshot of LEE solution $\pi'(t)$ obtained with physical source $f_{1z}(t, \pm\Delta\omega)$

(b) Snapshot of LEE solution $\pi'(t)$ obtained with source $f_{2z}(t, \pm\Delta\omega)$

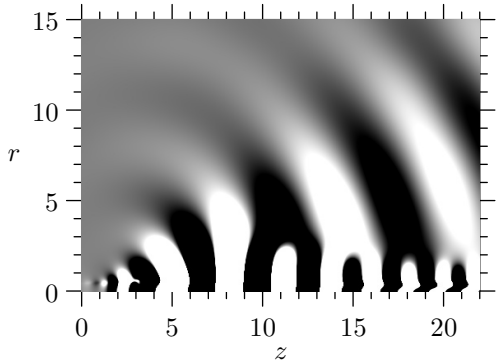

(c) Snapshot of DNS solution $\pi(t, \pm\Delta\omega)$

Figure 5: Comparison of radiating pressure solutions obtained by solving the LEE with physical source f_{1z} (a) and source f_{2z} (b), with the DNS solution (c). The contour scale ranges from $-1 \cdot 10^{-5}$ (black) to $1 \cdot 10^{-5}$ (white).

IV. Conclusion

For a homentropic flow, the physical sound sources can be expressed in terms of the non-radiating parts of the density and momentum density fields. These non-radiating parts are obtained by removing the radiating components in the Fourier domain. The dominant source term involves the non-radiating density and axial momentum density. As we expect, the sound sources have the same frequency content and amplitude as the radiating field. These physical properties are not satisfied by the sound sources that are based on acoustic analogies. This suggests that using the sound sources defined in the present paper should help us understand the physical mechanism of aerodynamic sound generation. The method presented in this paper can be extended to more complex flows by using a more general form of the energy equation.

Acknowledgements

We are indebted to Dr. Victoria Suponitsky and Professor Neil Sandham, who carried out the DNS simulation used in this paper. We would like to thank Professor Paul White and Drs. Gwénaël Gabard and Peter Jordan for many useful discussions. This project is funded by the Engineering and Physical Sciences Research Council under grant EP/F003226/1. The authors also gratefully acknowledge Rolls-Royce plc for their financial support.

References

[1]Goldstein, M., "A generalized acoustic analogy," *Journal of Fluid Mechanics*, Vol. 488, 2003, pp. 315 – 33.

[2]Goldstein, M. E., "On identifying the true sources of aerodynamic sound," *Journal of Fluid Mechanics*, Vol. 526, 2005,

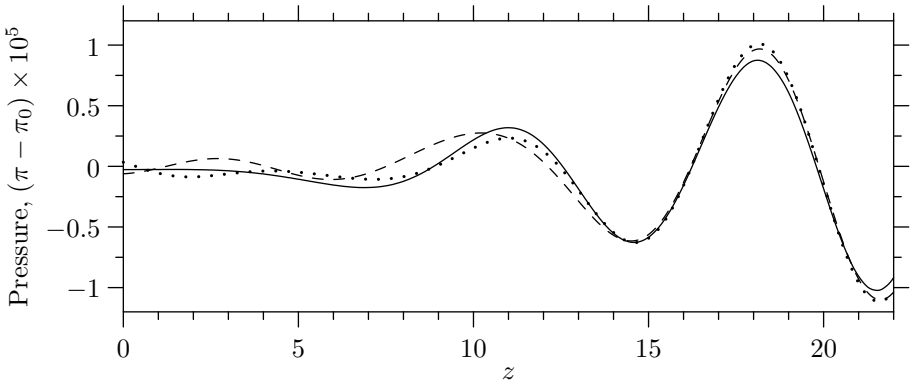

Figure 6: Profiles along $r = 10$ of radiating pressure solutions obtained by solving the LEE with physical source f_{1z} (dashed) and source f_{2z} (dotted). The solid line represents the DNS solution at frequency $\omega = 1.2$.

pp. 337 – 347.

[3]Sinayoko, S., Agarwal, A., and Hu, Z., "On separating propagating and non-propagating dynamics in fluid-flow equations," *AIAA paper 2009-3381*, 2009.

[4]Crighton, D. G., "Basic principles of aerodynamic noise generation," *Progress in Aerospace Sciences*, Vol. 16, 1975, pp. 31–96.

[5]Goldstein, M., *Aeroacoustics*, McGraw-Hill International Book Co., 1976.

[6]Lilley, G., "The Generation and Radiation of Supersonic Jet Noise. Vol. IV - Theory of Turbulence Generated Jet Noise, Noise Radiation from Upstream Sources, and Combustion Noise. Part II: Generation of Sound in a Mixing Region," *US Air Force Aero Propulsion Lab., AFAPL-TR-72-53, July*, 1972.

[7]Stromberg, J., McLaughlin, D., and Troutt, T., "Flow field and acoustic properties of a Mach number 0.9 jet at a low Reynolds number," *Journal of Sound and Vibration*, Vol. 72, No. 2, 1980, pp. 159–176.

[8]Suponitsky, V. and Sandham, N. D., "Nonlinear mechanisms of sound radiation in a subsonic flow," *AIAA paper 2009-3317*, 2009.

[9]Guizar-Sicairos, M. and Gutiérrez-Vega, J., "Computation of quasi-discrete Hankel transforms of integer order for propagating optical wave fields," *Journal of the Optical Society of America A*, Vol. 21, No. 1, 2004, pp. 53–58.

[10]Tam, C. and Webb, J., "Dispersion-relation-preserving finite difference schemes for computational acoustics," *Journal of Computational Physics*, Vol. 107, No. 2, 1993, pp. 262 – 81.